Taylor & Francis
Taylor & Francis Group

Canadian Metallurgical Quarterly

The Canadian Journal of Metallurgy and Materials Science

ISSN: (Print) (Online) Journal homepage: https://www.tandfonline.com/loi/ycmq20

Machinability of extruded and multi-directionally hot forged eco-friendly brass alloys

Nima Zoghipour, Emre Tascioglu & Yusuf Kaynak

To cite this article: Nima Zoghipour, Emre Tascioglu & Yusuf Kaynak (2023): Machinability of extruded and multi-directionally hot forged eco-friendly brass alloys, Canadian Metallurgical Quarterly, DOI: 10.1080/00084433.2023.2214980

To link to this article: https://doi.org/10.1080/00084433.2023.2214980

Published online: 22 May 2023.

Submit your article to this journal

Article views: 28

View related articles

View Crossmark data

Full Terms & Conditions of access and use can be found at
https://www.tandfonline.com/action/journalInformation?journalCode=ycmq20

CANADIAN METALLURGICAL QUARTERLY
https://doi.org/10.1080/00084433.2023.2214980

Check for updates

Machinability of extruded and multi-directionally hot forged eco-friendly brass alloys

Nima Zoghipour[a,b], Emre Tascioglu[a] and Yusuf Kaynak[b]

[a]Torun Bakır Alaşımları Metal Sanayi ve Ticaret A.Ş., Kocaeli, Turkey; [b]Department of Mechanical Engineering, Marmara University, Goztepe Campus, Istanbul, Turkey

ABSTRACT

Brass alloys assign a considerable portion of the industrial components' material due to their outstanding characteristics. These materials are manufactured using hot forging or extrusion techniques, according to the application for different purposes. In this work, the metallographic and mechanical characteristics of three environmentally friendly brass alloys – CuZn40Pb2 (CW617N), CuZn38As (CW511L) and CuZn21Si3P (CW724R) – extruded and multi-directionally hot forged have been examined. By focusing on the flat bottom drilling operation, the effects of the process and type of alloying have been investigated. The examination has been accomplished on experimental data about tensile strength, impact fracture energy, cutting forces, entrance and exit burr diameters, as well as hole quality. The findings demonstrate that the most crucial criteria impacting the machining outcomes are the presence of limited Pb element and material microstructural phases, their content and mechanical characteristics, as well as the type manufacturing process.

ARTICLE HISTORY
Received 17 March 2023
Accepted 3 May 2023

KEYWORDS
Extrusion, hot forging, eco-friendly brass alloys, lead-free brass alloy, twinning, machinability

Introduction

Brass alloys are indispensable in many industrial applications, particularly pumping systems and water treatment works, because of their superior formability, high specific strength, elastic modulus, hardness, good wear, corrosion resistance and recyclable nature [1]. The final brass products are made from either hot forged specimens or the machining of extruded bars, as shown in Figure 1, depending on their use and the necessary properties and functioning. Several researchers [2–9] have investigated various alloying elements for brasses to improve the material behaviour. Owing to the demonstrated improvement in machinability caused by lower cutting forces, torques, friction, tool wear, etc., lead is one of the most important constituents in traditional brass alloys. Nonetheless, the virulent and poisonous nature of lead has led organisations such as ROHS and EUPA to accept and publish stringent legislation for the use of this element in pumping and drinking water systems [10,11]. As a result, new brass varieties in the low-lead and lead-free alloy categories have been developed.

The extremely excellent chips with discontinuous tiny forms are a defining characteristic of cutting the leaded brass [12]. By utilising Auger electron spectroscopy, Stoddart et al. [13] demonstrated the development of a thin lead coating on the chip's side that rubs up against the cutting tool. They brought out that the formed layer results in lubrication, cooling of the cutting edge and reduction of forces. The generated friction in the machining of leaded and lead-free brass was carried out by Gane [14] by cutting and sliding experiments. The friction stress of the lead-free brass was double that of the leaded brass, according to the findings of his experiments. According to certain researchers [15–18], lead's low melting point enhances machinability. It is important to remember that lead's lubricating qualities, including thermal softening and earlier physical changes, are all temperature dependent.

Using powder metallurgy, Imai et al. [19]'s goal was to create lead-free, improved-machinability brass that was distributed with graphite particles. Schultheiss et al. [20] investigated the machinability of CuZn21Si3P as opposed to leaded brasses in longitudinally turning operation. The machinability of three lead-free brass alloys, CuZn42, CuZn38As and CuZn36, was compared with leaded brass CuZn39Pb3. Their findings indicated that CuZn21Si3P could not be turned using cutting tools. The cutting force and surface roughness in the operation of the turning mode were studied by Toulfatzis et al. [21]. Using the Taguchi approach, they made an effort to optimise the cutting speed, depth of cut, feed

CONTACT Nima Zoghipour nima.zoghipour@gmail.com
© 2023 Canadian Institute of Mining, Metallurgy and Petroleum

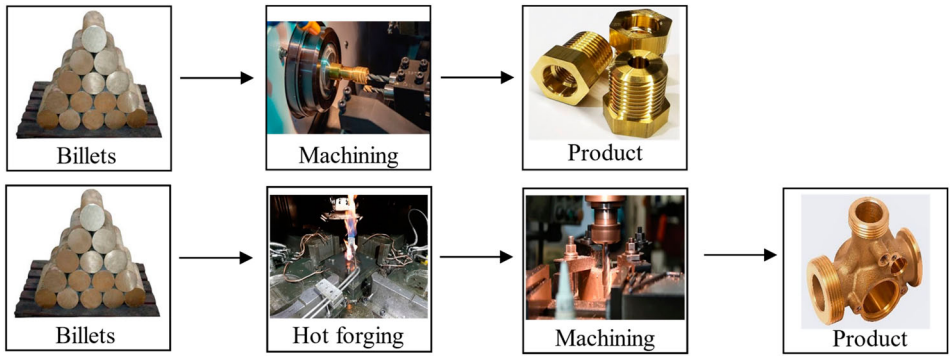

Figure 1. Manufacturing process steps for a final brass product: (a) extruded, and (b) hot forged.

rate and alloy. A comparison of the machinability of a conventional free-machining leaded alloy and brass alloys with reduced lead concentration was conducted by Johansson et al. [22], focusing on burr development, differences in cutting forces and cutting resistance. By their findings, leaded brass has better machinability than alloys with lower lead contents. The cutting force and chip formation in drilling and turning lead-free brass alloys were assessed by Aytekin [23]. He emphasised the impact of the geometry of the cutting tool on machinability. He found that turning lead-free alloys produced larger cutting forces than turning leaded alloys. In lead-free brass, micro-drilling was investigated by Kato et al. [24]. They focused on the effects of web thinning, the helix angle and the nick geometry on chip evacuation. By taking into account dimensional precision, hole quality, subsurface properties such microhardness and microstructure, Zoghipour et al. [25] assessed the surface integrity of specimens of lead-free brass that had been machined. They developed an artificial neural network model for drilling hot-forged lead-free brass alloys using a form-cutting tool in another work [26]. They employed genetic algorithm-based optimisation techniques to improve the machining process responsiveness and copper content while concentrating on the cutting forces, dimensional accuracy and surface quality of the holes.

Considering the developing of eco-friendly brass alloys as alternatives for conventional leaded ones, besides the complex shaped geometries of the components, the light weight of the machinability term becomes crucial to overcome the manufacturing requirements and customer demands as well as the cost reduction. Therefore, in this research, three types of most used brasses in the EUA7038 list; namely, leaded (CW617N), low-leaded (CW511L) and without lead (CW724R) brasses as extruded and forged specimens have been inspected in terms of metallographic; microstructures, micro-hardness, mechanical; tensile strength, impact fracture energy tests, machinability; cutting forces, torques, entry and exit burr heights, surface roughness. Through all holes were drilled in the extruded and forged specimens, the machinability has been assessed.

Experimental methodology

Different types of EN 12164 brass alloys comprised of leaded CuZn40Pb2, low-lead CuZn38As and lead-free CuZn21Si3P were selected to be investigated in this research paper. The chemical composition of the materials has been extracted through spectrum analysis as illustrated in Table 1. To perform a comprehensive comparison of the extruded and hot-forged brass alloy metallurgical and mechanical properties, half of the materials have been hot forged under a designed closed-die system. The billet dimensions were 35 and 200 mm in diameter and length, respectively. The hot forging operation was carried out at 730 ± 10 °C with a rate of 11 stroke min^{-1} under a 165 ton of press load in a Hydromec 550 eccentric press machine. Furthermore, specimens by the ASTM E8/E8M tensile test standard for metallic materials have been hot forged at 730 ± 10 °C with 70 tons of press with a rate of 9 stroke min^{-1}. The microstructural analysis of the mentioned brass alloys was carried out using SEM (Scanning electron microscope). The hardness of the materials has been measured by MHVD 1000 IS microhardness tester under 25 g applied load for 10 s. The impact Charpy tests have been executed with V-notched specimens according to ASTM E23 standards at room temperature. Flat bottom drilling experiments were carried out at feed rates of 500, 600, 700 mm min^{-1} and cutting speed of 125 m min^{-1} on Fanuc Robodrill α−D21LiB5 CNC machine under external cooling flood conditions. The cutting tool was a two-fluted YG1, X-Coated carbide dream flat bottom drill with D1, D2 = 8 mm, L1 = 34 mm and L2 = 70 mm as demonstrated in Figure 2. The cutting forces and torques have been measured using Kisteler dynamometer type 9129AA and the resultant of the cutting forces and

Table 1. The chemical composition of the studied materials.

Composition	Cu	Pb	Al	Fe	As	Mn	Ni	Sn	S	Cd	P	Si	Sb	Mg	Bi	Zn
CW617N	57.433	1.703	0.011	0.099	0.007	0.006	0.027	0.068	0.002	0.001	0.004	0.004	0.014	0.001	0.003	40.610
CW511L	62.104	0.156	0.005	0.005	0.010	0.100	0.008	0.004	0.070	0.002	0.001	0.002	0.004	0.004	0.003	37.522
CW724R	76.049	0.062	0.003	0.023	0.000	0.000	0.005	0.007	0.002	0.001	0.054	2.900	0.003	0.000	0.000	20.884

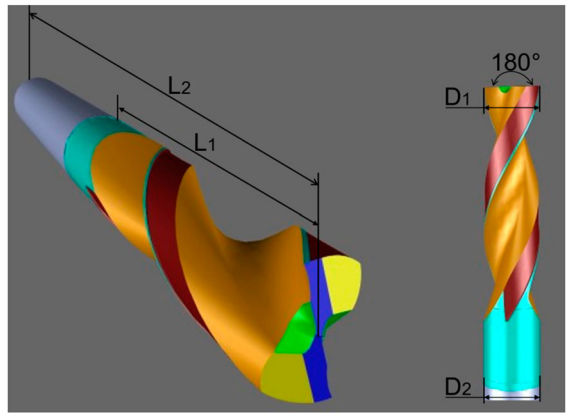

Figure 2. The used flat bottom drill in this study.

torque values is reported. The burr heights and surface roughness have been measured using a Mituoyo SV-3000 contracer. The experiments were comprised of three various types of brass alloys manufactured with two different methods using diverse machining parameters. All the experiments were executed with three repetitions and the average is reported in the article. The experimental setup is shown in Figure 3.

Results and discussion

In this section, the comparison between the machinability of six materials cutting forces, burr sizes, surface roughness as well as surface and sub-surface integrity issues has been discussed by concentrating on the microstructure, microhardness, tensile strength and impact fracture toughness.

Machining tests

To make a comparison among the obtained results comparable, axial cutting forces and torques are employed for the materials with various feed rates. The cutting forces in the axial orientation are shown for the materials at $V_f = 700$ mm min^{-1} in Figure 4. In a mindful look at the measured force graphs, it is seen there is a salient peak at the entrance to the work material for low-lead and lead-free brass alloys illustrating the higher subjective forces on the cutting tool. It is thought that these peaks are because of the shearing energy, hardness, tool localisation and cutting followed by ductile fracture.

Figures 5 and 6 demonstrate the variations of the thrust force (*Fz*) and torques (*Mz*) with respect to the cutting conditions (i.e. the brass alloy type and the feed rate). From these two figures, the similarities and differences in flat bottom drilling of extruded and forged brass alloys are observed and compared as follows:

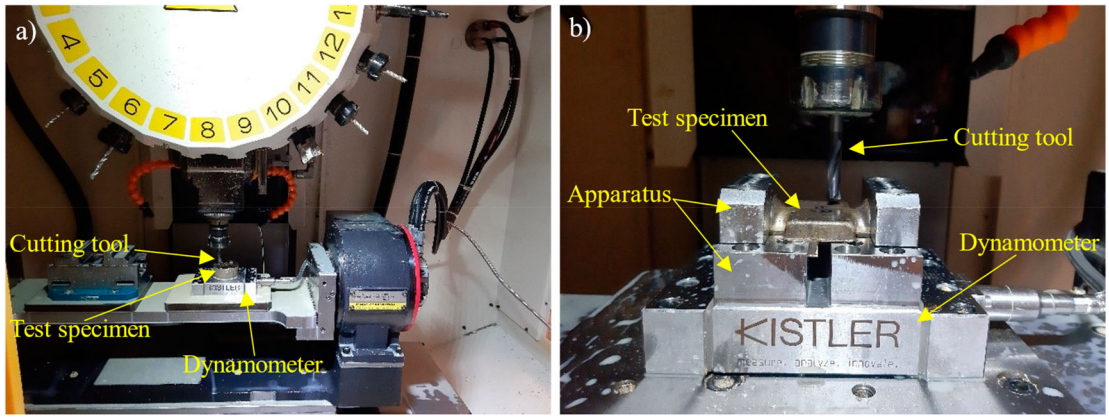

Figure 3. The experimental setup: (a) extruded and (b) forged specimen.

(1) For all the extruded and forged brass alloys: an increase in the feed rates has led to an augmentation in both the thrust force and torque due to the extension in the contact area between tool take face and work material.
(2) The highest cutting force and torque value have been observed for forged CW511L as 529.5 and 5.7 N.m, respectively. However, the lowest values were 245.4 and 2.1 N.m for extruded CW617N. It is seen that under the same cutting conditions, the cutting force and torques in the machining of CW511L are higher than those in CW724R and CW617N.

The microstructure of the extruded and forged CW617N, CW511L and CW724R brass alloys is exhibited in Figure 7. The light grey colours represent the α phase, while the β phases are seen in pale grey for CW617N and CW511L. The combinations of α, γ (small phases at grain boundaries) and κ phases are observed for CW724R. It is significant to note that the lattice structure of α, β, γ and Si-rich κ phases are FCC (Face centred cubic), BCC (Body centred cubic), FCC and hexagonal, respectively. Therefore, it is anticipated to observe an increase in the brittlely but more

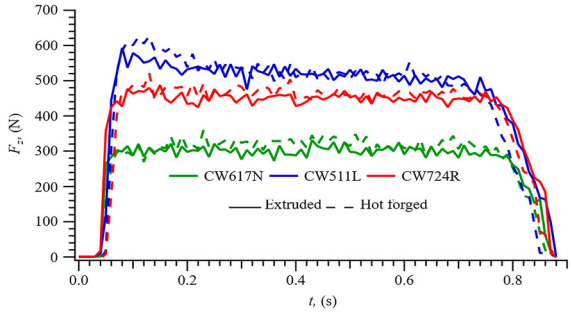

Figure 5. The measured cutting forces of the studied brass alloys.

durability with the rise in the β phase in CW617N and CW511L regarding the higher number of slip systems and dislocation lattice friction stresses as compared to α phase which is FCC. In addition, due to the convenient motion of dislocations in HCP (Hexagonal Close-Packed) because of three slip systems as compared to FCC and BCC, it is foreseen for CW724R to demonstrate brittlely.

As a subsequence of multi-directional hot forging, the β phase has increased from 46% to 51% for CW617N. This rate was measured from 5% to 17% for CW511L. This augmentation and elongation can be

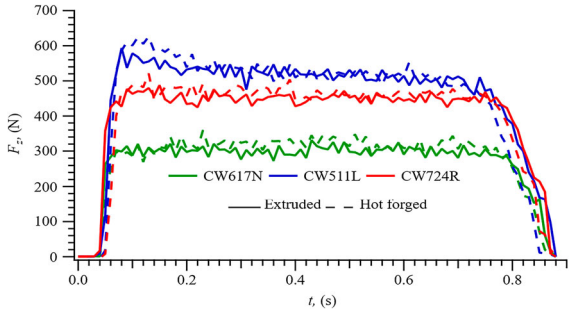

Figure 4. The measured thrust forces at $V_f = 700$ mm min^{-1}.

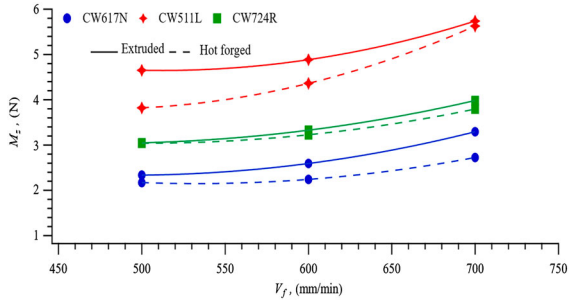

Figure 6. The measured torques of the studied brass alloys.

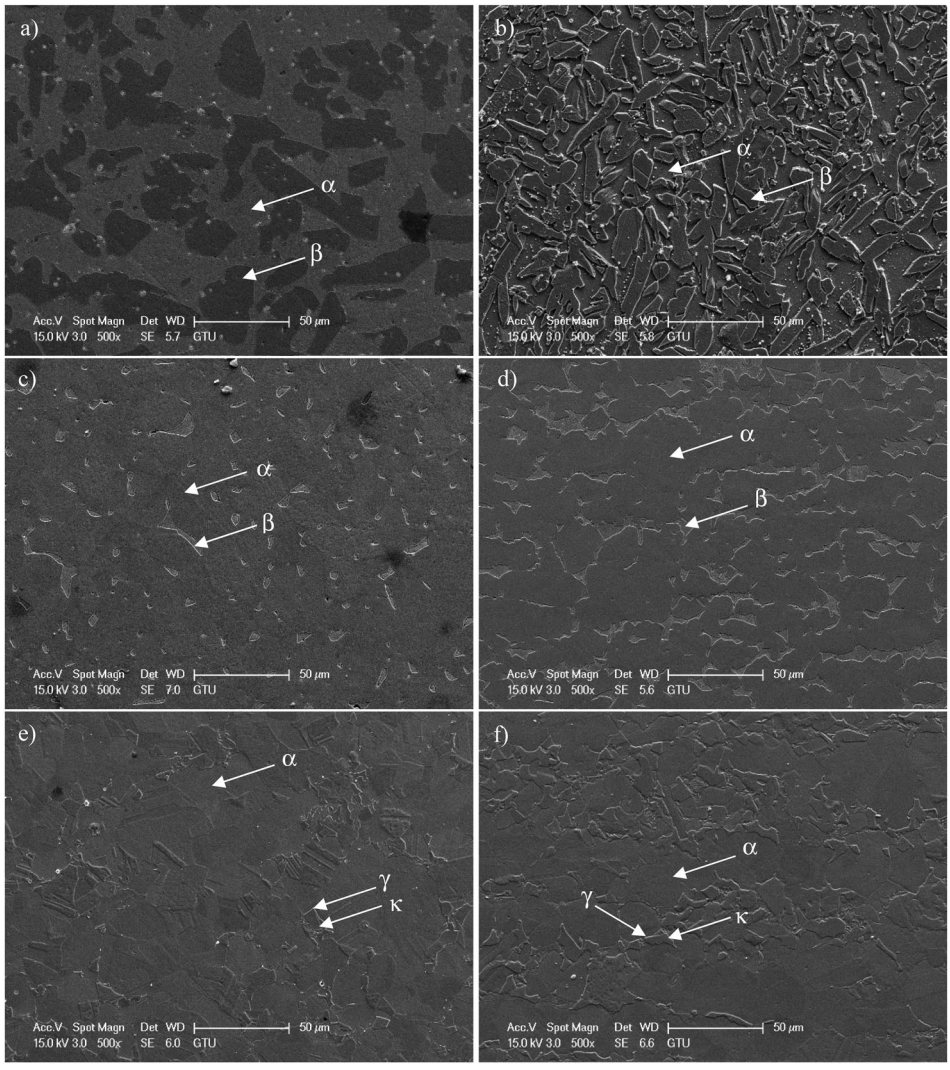

Figure 7. SEM images of etched brass alloys microstructure: (a) extruded CW617N, (b) forged CW617N, (c) extruded CW511L, (d) forged CW511L, (e) extruded CW724R and (f) forged CW724R.

attributed to the superplastic deformation behaviour of the β phase in the forging process. According to [27–29], at high temperatures and low strain rates of dual brasses, α phase exposes recrystallisation, whereas β experiences superplastic deformation. For CW724R, the κ and γ phases have boosted from 16% to 19%. Consequently, looming up of the κ phase and considering the lower percentages of γ phases as compared to κ phases, it seems to be feasible to neglect them to conclude that material will obtain more brittlely by forging.

The highest measured microhardness value of the extruded and forged brass alloys is 138.9 HV for forged CW724R, while the lowest one was 92.1 HV for extruded CW511L. The microhardness of the CW617N, CW511L and CW724R has increased 12.8%, 11% and 17.5%, respectively. As demonstrated in the previous section of this paper, the β phase percentage has been augmented by hot forging. This increase can be attributed to the rise in the BCC structure of the β phase in CW617N and CW511L. The microstructure images of the specimen have proved that the α phase of CW724R decreases by forging which means the increase of the harder phases such as κ as well as the existence of Si elements in the chemical composition leading to a harder surface. Furthermore, to determine the process parameter effect when drilling with a flat bottom drill, the microhardness of the sub-surface has been measured at different depths. The lowest microhardness values were measured for hot forged and extruded CW511L materials as equal to 102.3 and 92.1 HV at the depth of 300 μm, respectively. However, the highest ones were 148.45 and 143.95 HV at the machined surface for hot forged and extruded CW724R materials, respectively. It is well known that plastic deformation and material drag are executed in the orientation of the cutting direction during the

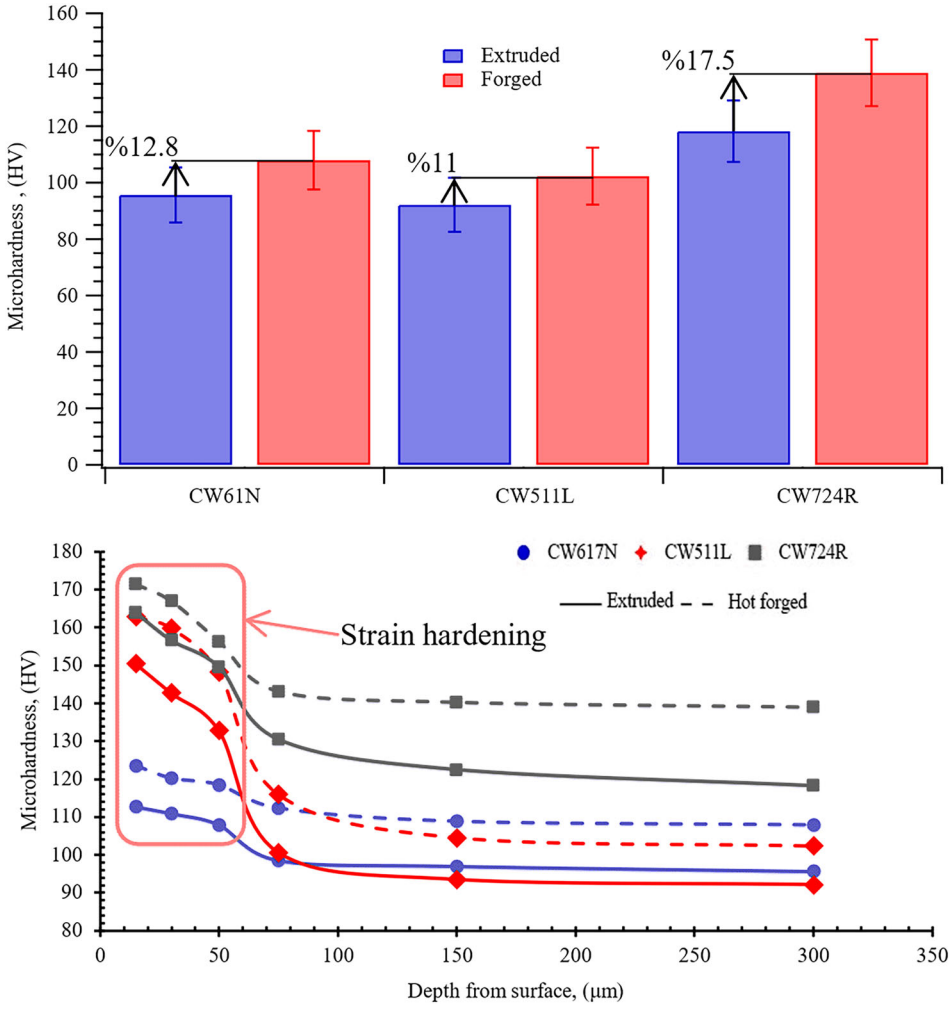

Figure 8. The measured microhardness values of the studied brass alloys: (a) before machining and (b) after machining.

machining of metals. Moreover, the microhardness of the surface and sub-surface up to a definite depth intensifies due to the generated strain hardening on the materials [25,30]. This occurrence is reliant upon the thermomechanical state of the formed surface including cutting condition, tool geometry and its wear. It is realised that the higher mechanical load brought about by a higher feed concludes with a deeper and higher strain hardening [31,32]. The shear interaction between the tool and the workpiece during machining serves as the reason for the high-temperature gradient. The consequence is localised heating and plastic deformations in the subsurface region, which might contribute to mechanical, thermal and metallurgical modifications. A reduction in the microhardness with respect to the depth in the sub-surface was observed because of the strain hardening as displayed in Figure 8. Thereafter, the microhardness has altered to the measured value before machining.

The subsurface region has substantial deformation due to increased shear in the cutting direction, as seen by SEM images of the machined surface and sub-surfaces are demonstrated in Figure 9. The harsh surface and sub-surface deformations, irregularities as well as the formation of twinning have been shaped in CW511L and CW724R brass alloys due to the stain hardening and plastic deformation during machining. The number and thickness of deformation twins are significantly higher in CW511L as compared to CW724R. However, no twinning and sub-surface deformation unaffected by the machining conditions was observed for CW617N, and the machined surface is smooth as the bulk material. Therefore, it can be concluded that the escalation in the twin number and its density leads to the expansion in the strain-hardening rate which is all in agreement with the obtained measurement results.

The forged test materials have demonstrated higher thrust forces and torques as compared to extruded ones. This is due to the higher hard β phase percentage which is inherently associated with the chip breakability and machinability [33]. According to [21], in the machining of leaded brass alloys, the distribution of

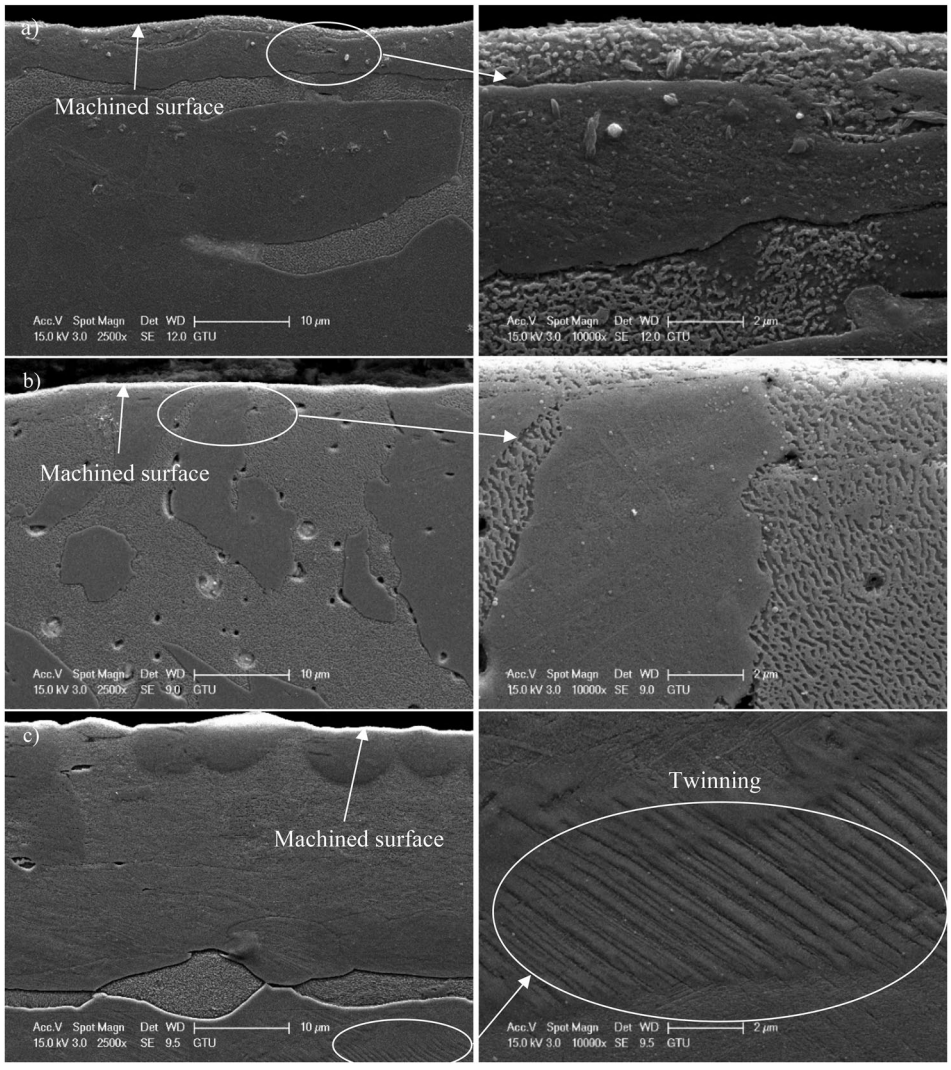

Figure 9. The deformation on the sub-surfaces of the machined holes: (a) extruded CW617N, (b) forged CW617N, (c) extruded CW511L, (d) forged CW511L, (e) extruded CW724R and (f) forged CW724R.

the Lead element among the grain boundaries is the fundamental controlling criteria for chip breaking. However, the shear band formation and micro-crack generation in low-lead and lead-free brasses are related to the β phase [21]. The presence of Pb element brings about lower cutting forces by keeping more lubricant on its surface and subsequently decreasing the wear or friction during the contact [22,23,34]. Additionally, the melting point of CW724R and CW511L are 600°C and 900°C, respectively [35]. Consequently, softening during machining can be one more justification for the lower cutting forces of CW724R as compared to CW511L at high temperatures in machining. Moreover, in a comparison of the machining responses with tensile test results, it is seen that the measured thrust forces and torques are CW511L > CW724R > CW617N not completely linear dependent on the existence of Pb in the composition. This is appertaining to the lower strain rates (2 mm per min rate of elongation in this paper) as compared to the generated strain rates in machining resulting to exhibit different properties. Long and lamellar chips were observed during the machining tests of CW511L. The visual chip sizes of CW724R were smaller. In contrast, discontinuous, short and easily broken chips were formed for CW617N. This result was also discussed in [36,37]. They also have brought out the ductility of the leaded brasses is lower than lead-free brasses. This lower ductility results in discontinuous and small chip formation as we observed in this research. Hofmann et al. [37] have explained the differences in ductility behaviour for leaded and lead-free at high strain rates.

Burr sizes

Burr height in the flat bottom drilling operation is a result of the materials' plastic deformation behaviour

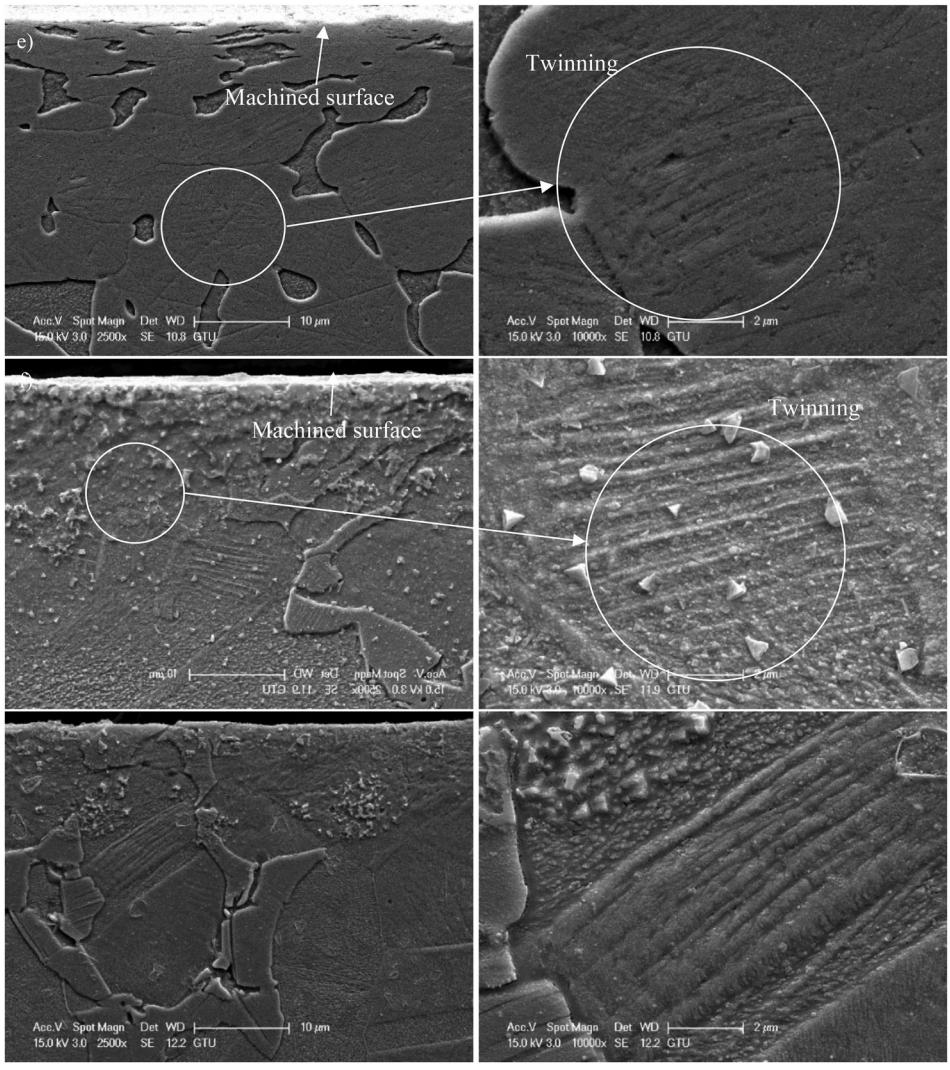

Figure 9 *Continued*

including elongation and fracture. In other words, burr formation during a machining process is an undesired feature associated with material ductility and strains [32,36–40]. Roll-over type formed burrs are observed on the extruded and forged specimens. The average measured entry and exit burr heights results are given in Figure 10. The highest formed entry burr height was measured on forged CW511L as 72.976 µm at 700 mm min^{-1}, while the lowest one was obtained in forged CW724R as equal to 21.92 µm at 500 mm min^{-1}. For the case of the exit burrs, the highest height was for extruded CW511L as 168.696 µm at 700 mm min^{-1}. However, the lowest burr size was measured for forged CW724R as 73.993 µm at 500 mm min^{-1}.

The extruded and forded CuZn40Pb2, CuZn38As and CuZn21Si3P specimens were subjected to tensile strength tests at 2 mm per min rate of elongation. The stress–strain curves of the three types of brass alloys are demonstrated in Figure 11. As it is seen the forged specimens have demonstrated a semi-brittle behaviour during the tests by sudden rupture without necking. Moreover, their plastic region is small as compared to the extruded specimens. The measured yield strength of the studied brass alloys is shown in Figure 12. The highest yield point stress was inspected for the forged CW724R as 387 MPa. However, the lowest one was for the extruded CW511L bar as equal to 136 MPa. It is seen that the yield stress increased 58%, 52%, 72% for CW617N, CW511L and CW724R by forging, respectively. The highest ultimate tensile strength was observed for forged CW724R as equal to 550.9 MPa whereas the lowest one was seen for extruded CW511L with 366.6 MPa. These results can be attributed to the double working under tension compacts on the metal and the formation of a dense and refined grain structure gained by twice applied high pressures during rod extrusion and forging [26] as well as phase transformation in the structure. Although the obtained

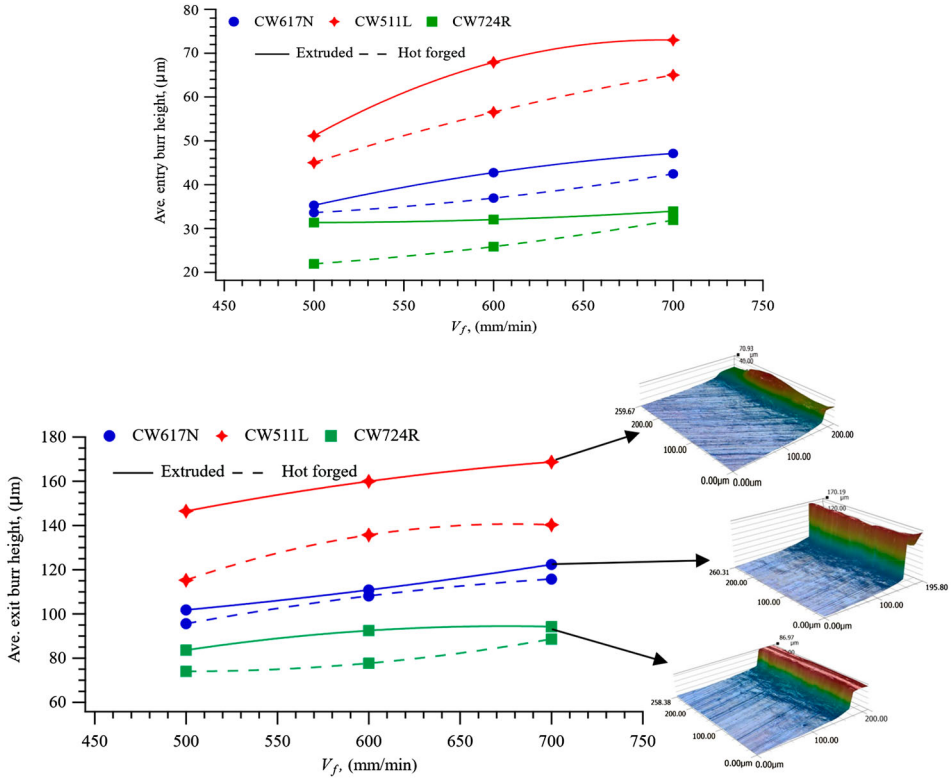

Figure 10. The average measured burr height for the studied materials: (a) entry and (b) exit.

results in this paper for the extruded bar of CW511L are lower than [41] reports, but they are very close to the catalog values of the company [35] which the brass alloys have been provided in this study. Furthermore, the calculated elastic modulus for the mentioned materials is all in the range of 78–85 GPa confirms the carried-out test results with the raw materials provider's catalog values.

To determine the required energy to fracture the extruded and forged brass alloy under dynamic loads, impact Charpy test was used. In this paper, the impact Charpy tests have been carried out with V-notched specimens according to ASTM E23. The average of two measurements of the notched impact energy is given in Table 2. The highest toughness value was measured for forged CW724R as equal to 26.51 kJ.

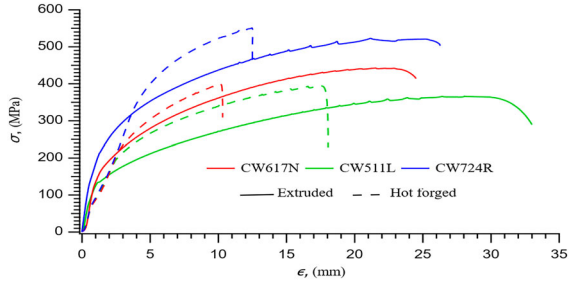

Figure 11. Stress–strain curves of the studied materials.

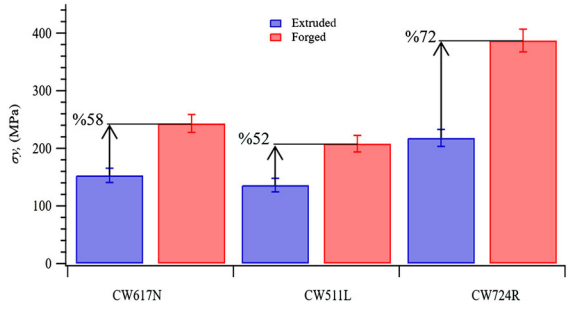

Figure 12. The measured yield strength of the studied brass alloys.

However, the lowest one was observed for extruded CW511L as 86.26 KJ. It is an event to note that the absorbed energy amount has been decreased for the test materials by hot forging. In other words, the plastic deformation property of the materials has been reduced by forging. This result confirms the obtained results on the tensile strength tests. The fractographic images of

Table 2. The toughness results of the studied brass alloys.

	Extruded bar	Forged
CW617N	35.71	27.41
CW724R	29.97	26.51
CW511L	86.26	57.6

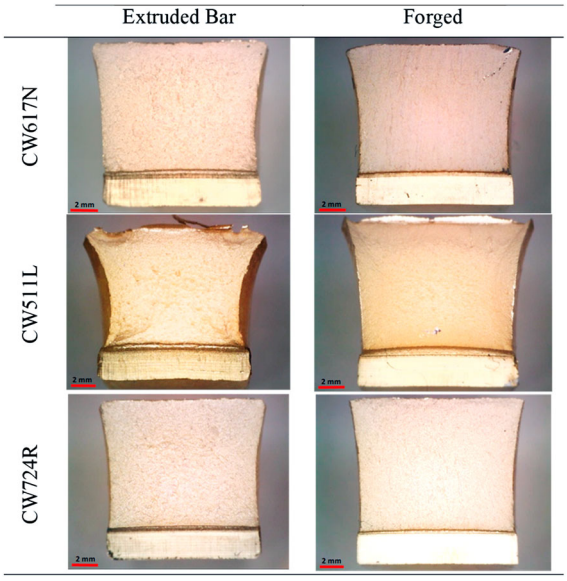

Figure 13. The fractographic images of the impact fractures of the studied brass alloys.

Table 3. The first mode fracture toughness results of the studied brass alloys.

	Extruded bar	Forged
CW617N	429.54	682.20
CW724R	612.02	1086.47
CW511L	381.81	583.94

the impact fractures are exhibited in Figure 13. As it is seen, an astonishing deformation in the visual shape of CW511L is achieved which exposes that the material has experienced higher strains before fracture. This shape and absorbed energy value are in agreement with [41]. However, the shape deformation in CW724R and CW617N is lower than CW511L due to movement restriction of the molecules and lower required energy for breaking the nuclear bonds, crack initiation and thus lower absorbed energy. The first mode fracture toughness values of the test specimens have been calculated by Equation (1) and the results have been reported in Table 3.

$$K_{IC} = Y\sigma_y\sqrt{\pi a} \tag{1}$$

where K_{IC}, Y, σ_y and a are the first mode fracture toughness, geometric constant, yield stress and crack/notch length, respectively [42–44].

The surface area change for extruded and forged CW617N was measured as 110.26% and 104.52% using the Digimizer program, respectively. This rate was 124.25%, 113.56%, 106.19% and 104.43% for extruded and forged CW511L and CW724R, respectively.

As a result of material ductility and resistance to plastic deformation, it is seen that the measured burr height results are in agreement with the fracture toughness values of this paper. The higher impact fracture energy, the higher shape deformation and burr heights are achieved because of the explained reasons in the previous sections of this research.

Surface roughness

The arithmetic surface roughness (Ra) values of the test specimen are exhibited in Figure 14. The highest surface

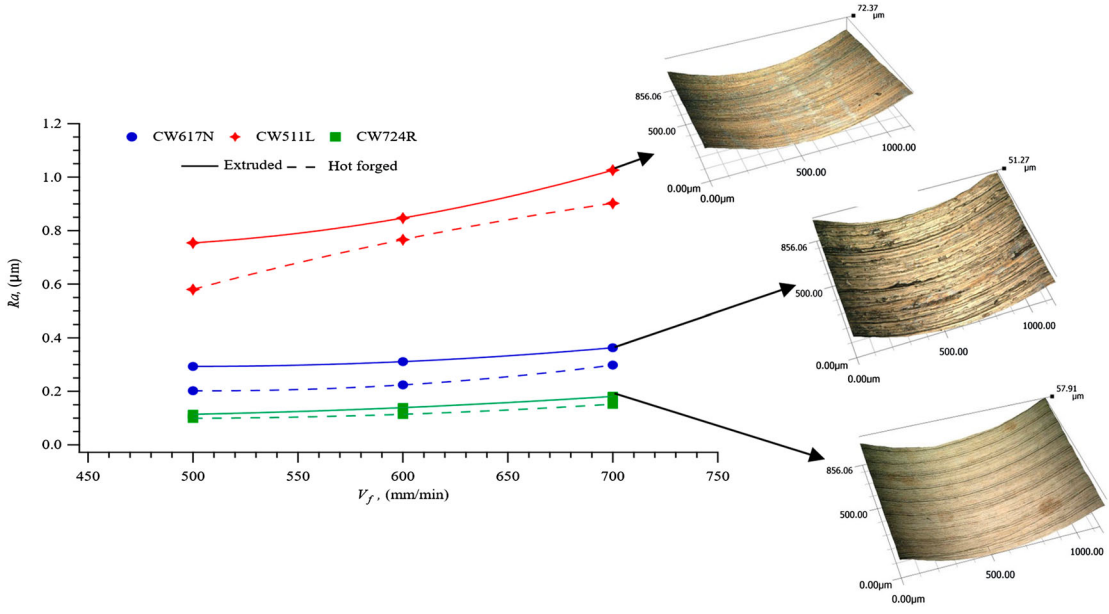

Figure 14. The average measured surface roughness for the studied materials.

roughness was measured for extruded CW511L as 1.026 μm. However, the lowest one was observed for forged CW724R as 0.099 μm. It is seen that higher surface qualities are achieved by forging the specimens. This might be due to the harder surfaces obtained by phase transmissions during the hot forging process. Furthermore, the authors believe that higher surface roughness of the leaded brass as compared to the lead-free one might be due to distributed Pb elements in the grain boundaries of CW617N resulting in an inhomogeneous surface.

Conclusion

In this research, interaction analysis of microstructural, mechanical and machinability properties of extruded and multi-directionally hot forged three different types of eco-friendly brass alloys were investigated in a comparative study. The evaluation of the machinability of the specimens was carried out based on the cutting forces, torques, entry, exit burr heights and surface quality of the drilled holes. It has been attempted to clarify the machining outputs based on the microstructural and mechanical properties depending on the manufacturing process type. Therefore, the below-given results were achieved.

The existence of the Pb element in the chemical composition of the brass alloys results in lower cutting forces and torques. However, it was observed that this approach is not always valid considering the burr sizes and surface quality. But study observations confirmed that the chip breakability and also chip pull out improve while machining both extruded and forged leaded brass alloys.

The main criteria influencing the machining outputs are the material microstructure and ductility. For this reason, the manufacturing method plays a significant role in these properties due to the phase transformations, promotions and grain size changes. It was seen that it can raise the yield stress of the components by 58%, 52% and 72% for CW617N, CW511L and CW724R, respectively with the hot forging process. Furthermore, hot forging has reduced the quantity of absorbed energy for the test materials. Forging has thereby decreased the materials' ability to deform plastically. It was observed that the induced plastic strain is more pronounced in the studied specimens' subsurface area, and leaded brass exhibits only slight changes in plastic strain intensity when compared to low-lead and lead-free brass. Considering the surface and subsurface hardness measurements, intensity of subsurface deformation in leaded brass is by far lower as compared to low-lead and lead-free brass samples. The authors propose conducting research on grain deformation and its orientation variation analysis in the subsurface region as a follow-up inquiry to the findings in the current work.

Primarily, although leaded types of brasses are being restricted by the published laws, it was observed that there are still a lot of milestones to be passed for a complete solution in high-quality component manufacturing of low-lead and lead-free brasses. Formability, cutting tool life, chip control, energy consumption and manufacturing costs are some factors that must be considered in parallel with the material development.

Acknowledgements

The authors thank TUBITAK (The Scientific and Technological Research Council of Turkey) for partially supporting this work under project number 118C069.

Disclosure statement

No potential conflict of interest was reported by the author(s).

Funding

This work was supported by TUBITAK: [Grant Number 118C069].

References

[1] Alagarsamy SV, Ravichandran M, Meignanamoorthy M, et al. Prediction of surface roughness and tool wear in milling process on brass (C26130) alloy by Taguchi technique. Mater Today. 2020;21(1):189–193. doi:10.1016/j.matpr.2019.04.219.
[2] Szyszkowski A. Les principaux laitons au plomb et leurs usages, Centre Belge d' Information du Cuivre, Publication no. 53/V, Symposium "Les laitons", 1973 (in French).
[3] Ragon R, Stucy M. Influence du plomb sur l'usinabilite´ des alliages cuivreux pour robinetterie. Fonderie—Fondeur d' Aujourd' hui. 1997;170:8–15.
[4] Saigal A, Rohatgi P. Machinability of cast lead free yellow brass containing graphite particles. AFS Trans. 1996;104:225–228.
[5] Whiting L, Newcombe P, Sahoo M. Casting characteristics of red brass containing bismuth and selenium. AFS Trans. 1995;103:683–691.
[6] Twarog D. Modified red brass with bismuth and selenium: research results. AFS Trans. 1995;103:451–461.
[7] Arnaud D. Composition and characteristics of copper alloys, 1989;12–16.
[8] French A. Improved free-machining leaded brass. J Inst Met. 1973;101:125–137.
[9] Le TP-J, Arnaud D. Influence des impuret´ es sur les proprietes des laitons. Fonderie. 1959;162:323–325.

[10] https://www.copper.org/applications/rodbar/pdf/A7038-brass-for-european-potable-water-applications.pdf.
[11] https://rohs.exemptions.oeko.info/fileadmin/user_upload/RoHS_Pack_9/Exemption_6_c_/Exemption_6c__2015-10-mitsubishi-shindoh-rohs.pdf.
[12] Williams JE, Smart EF, Milner DR. Metallurgy of machining 2. cutting of single-phase, 2-phase and some free machining alloys. Metallurgia. 1970;81(484):51–59.
[13] Stoddart CTH, Lea C, Dench WA, et al. Relationship between lead content of Cu–40Zn,: machinability, and svvarf surface composition determined by Auger electron spectroscopy. Met Technol. 1979;6(1):176–184. doi:10.1179/030716979803276435.
[14] Gane N. The effect of lead on the friction and machining of brass. Philos Mag A. 1980;43(3):545–566. doi:10.1080/01418618108240394.
[15] Wolfenden A, Wright PK. Role of lead in free-machining brass. Met. Technol. 1979;6(1):297–302. doi:10.1179/030716979803276697.
[16] Bjerke A, Hrechuk A, Lenrick F, et al. Thermodynamic modeling framework for prediction of tool wear and tool protection phenomena in machining. Wear. 2021;15:484–485. doi:10.1016/j.wear.2021.203991.
[17] Samandi M, Wise M. Machinability of copper based alloys. J INCRA Rep. 1989;1:110–115.
[18] Trent EM. Metal cutting and the tribology of seizure: III temperatures in metal cutting. Wear. 1988;128(1):65–81. doi:10.1016/0043-1648(88)90253-0.
[19] Imai H, Kosaka Y, Kojima A, et al. Characteristics and machinability of lead-free P/M Cu60–Zn40 brass alloys dispersed with graphite. Powder Technol. 2010;198(3):417–421. doi: 10.1016/j.powtec.2009.12.010.
[20] Schultheiss F, Johansson D, Linde M, et al. Machinability of CuZn21Si3P brass. Mater Sci Technol. 2016;32(17):1744–1750. doi: 10.1080/02670836.2016.1189199.
[21] Toulfatzis AI, Pantazopoulos GA, David CN, et al. Machinability of eco-friendly lead-free brass alloys: cutting-force and surface-roughness optimization. Metals (Basel). 2018;8(4):250. doi: 10.3390/met8040250.
[22] Johansson J, Persson H, Ståhl J-E, et al. Machinability evaluation of low-lead brass alloys. Proc Manuf. 2019;38:1723–1730. doi: 10.1016/j.promfg.2020.01.102.
[23] Aytekin K. Characterization of machinability in lead-free brass alloys, Degree Project In Materials Design And Engineering, Second Cycle, 30 Credits Stockholm, Sweden, 2018.
[24] Kato H, Nakata S, Ikenaga N, et al. Improvement of chip evacuation in drilling of lead-free brass using micro drill. Int J Automation Technol. 2014;8(6):874–879. doi: 10.20965/ijat.2014.p0874.
[25] Zoghipour N, Tascioglu E, Atay G, et al. Machining-induced surface integrity of holes drilled in lead-free brass alloy. Proc CIRP. 2020;87:148–152. doi: 10.1016/j.procir.2020.02.102.
[26] Zoghipour N, Atay G, Kaynak Y. Modeling and optimization of drilling operation of lead-free brass alloys considering various cutting tool geometries and copper content. Proc CIRP. 2021;102:246–251. doi: 10.1016/j.procir.2021.09.042.
[27] Padmavardhani D, Prasad YVRK. Characterization of hot deformation behavior of brasses using processing maps: part II. α brass and β brass. Metall Trans A. 1991;22A:2993–3001.
[28] Griffiths P, Hammond C. Superplasticity in large grained materialsSuperplasticite dans les materiaux a gros grainsSuperplastizität in materialien mit groβer korngröβe. Acta Metall. 1972;20:935–945.
[29] Callister WD, Rethwisch JRDG. Materials science and engineering, Wiley Binder Version ISBN: 978-1-118-47770-0.
[30] Ulutan D, Ozel T. Machining induced surface integrity in titanium and nickel alloys: A review. Int J Mach Tools Manuf. 2011;51(3):250–280. doi: 10.1016/j.ijmachtools.2010.11.003.
[31] Ståhl J-E. Metal cutting theories and models, Seco Tools, Diverse Production Materials Engineering, 2012.
[32] Johansson J, Bushlya V, Obitz C, et al. Influence of subsurface deformation induced by machining on stress corrosion cracking in lead free brass. Int J Adv Manuf Technol. 2022;122:3171–3181.
[33] Pantazopoulos G, Vazdirvanidis A. Characterization of microstructural aspects of machinable α-β phase brass. Microsc Anal. 2008;22:13–16.
[34] Tascioglu E, Zoghipour N, Sharif S, et al. Machining-induced surface integrity in brass alloys. Proc CIRP. 2022;108:654–659. doi: 10.1016/j.procir.2022.04.078.
[35] https://sarbak.com.tr/en/documents/alloys.
[36] Jaspers SPFC, Dautzenberg JH. Material behaviour in metal cutting: strains, strain rates and temperatures in chip formation. J Mater Process Technol. 2002;121(1):123–135. doi: 10.1016/s0924-0136(01)01227-4.
[37] Hofmann U, El-Magd E. Behaviour of Cu–Zn alloys in high-speed shear tests and in chip formation processes. Mater Sci Eng A. 2005;395(1–2):129–140. doi: 10.1016/j.msea.2004.12.030.
[38] Dhanke VD, Phafat NG, Deshmukh RR. Optimization of process parameters in drilling of AISI 1015 steel for exit burr using RSM and Taguchi. Int J Mech Eng Technol (IJMET). 2013;4(4):327–337.
[39] Ko SL, Lee JK. Analysis of burr formation in drilling with a new-concept drill. J Mater Process Technol. 2001;113(1–3):392–398. doi: 10.1016/S0924-0136(01)00717-8.
[40] Gillespie LK, Blotter PT. The formation and properties of machining burrs. J Eng Ind. 1976;98(1):66–74.
[41] Toulfatzis AI, Pantazopoulos GA, Paipetis AS. Fracture behavior and characterization of lead-free brass alloys for machining applications. J Mater Eng Perform. 2014;23:3193–3206.
[42] Wang CH. Introduction to fracture mechanics. Melbourne, Vic.: DSTO Aeronautical and Maritime Research Laboratory; 1996.
[43] Şar E. Tensile opening mode fracture toughness measurements and size effect investigations with Brazilian disc type rock specimens. Middle East Technical University; 2020.
[44] Doyle ED. Mechanisms of plastic instability in the machining of metals, 1974.